energies

MDPI

Article

Exploring Vinyl Polymers as Soft Carbon Precursors for M-Ion (M = Na, Li) Batteries and Hybrid Capacitors

Afshin Pendashteh, Brahim Orayech, Jon Ajuria, María Jáuregui and Damien Saurel *

Centre for Cooperative Research on Alternative Energies (CIC energiGUNE), Basque Research and Technology Alliance (BRTA), Alava Technology Park, Albert Einstein 48, 01510 Vitoria-Gasteiz, Spain; apendashteh@cicenergigune.com (A.P.); borayech@cicenergigune.com (B.O.); jajuria@cicenergigune.com (J.A.); mjauregui@cicenergigune.com (M.J.)

* Correspondence: dsaurel@cicenergigune.com

Received: 29 June 2020; Accepted: 10 August 2020; Published: 13 August 2020

Abstract: The viability of the sodium-ion batteries as a post-lithium storage technology is strongly tied to the development of high-performance carbonaceous anode materials. This requires screening novel precursors, and tuning their electrochemical properties. Soft carbons as promising anode materials, not only for batteries, but also in hybrid capacitors, have drawn great attention, due to safe operation voltage and high-power properties. Herein, several vinyl polymer-derived soft carbons have been prepared via pyrolysis, and their physicochemical and sodium storage properties have been evaluated. According to the obtained results, vinyl polymers are a promising source for preparation of soft carbon anode materials for sodium-ion battery application. In addition, their applicability towards Li-ion battery and hybrid capacitors (e.g., Li ion capacitors, LICs) has been examined. This work not only contrasts the carbonization products of these polymers with relevant physicochemical characterization, but also screens potential precursors for soft carbons with interesting alkali metal-ion (e.g., Na or Li, with an emphasis on Na) storage properties. This can stimulate further research to tune and improve the electrochemical properties of the soft carbons for energy storage applications.

Keywords: vinyl polymers; soft carbon; sodium storage; anode material; hybrid capacitor

1. Introduction

Li-ion batteries (LIBs) are currently the most advanced electrical energy storage devices, and are used in many applications (including smartphone and electric vehicles). However, they are not likely the ideal type of battery to meet the increasing demand of large-scale energy storage, since Li is a limited recourse (ca. 20 ppm in the Earth's crust), unequally distributed recourse (mainly found in South America), and is expensive [1,2]. This is further aggravated by high cost and scarcity/toxicity concerns of other LIBs components, such as Co-containing cathode materials. Accordingly, other alkali metal-ion batteries, especially sodium-ion batteries (SIBs), have recently attracted great attention as an alternative to LIBs owing to their potentially lower cost as being based on more abundant elements [1,3]. In fact, sodium is one of the most abundant elements in the Earth's crust, as well as being infinitely found in the oceans. In addition, there are other features that make SIBs highly interesting, such as the possibility of aluminum use (lighter and cheaper compared to copper) as the current collector in anode side without the concern of alloy formation (unlike in LIBs), and the fact that the electrode materials in SIBs are commonly Co-free. Many similar aspects in these two battery technologies will result in a quick SIB-transition to the market, thanks to all fabrication advances for LIBs made over the past two decades [4]. However, these similarities do not extend to the applicability of LIBs' electrode materials in SIBs—this is one of the main bottlenecks of SIBs commercialization. Graphite, however, (the most

used anode material in Li^+ rocking-chair batteries) does not fit into the picture for SIBs (e.g., with a suppressed reversible capacity of ≈30 $mAh{\cdot}g^{-1}$, due to unfavorable thermodynamic formation of graphite intercalation compounds, GICs) [3,5]. In contrast to graphite, disordered sp^2 carbons (e.g., hard and soft carbons) have attracted the most attention as the anode materials for SIBs [6]. In 1993, petroleum coke-based soft carbon (SC) was the first of its kind for which sodium insertion was reported with a limited capacity of a bit beyond 100 $mAh{\cdot}g^{-1}$ [7]. Later on, most of the research was focused on hard carbons (HC) as a result of the pioneer report by Stevens and Dahn, in 2000, who demonstrated a capacity of ≈ 300 $mAh{\cdot}g^{-1}$ [8]. Despite their higher specific capacity in comparison with SCs, HCs suffer from safety concerns arisen from their very low potential plateau (≤0.1 V vs. Na/Na^+) which may result in easily formation of sodium dendrites in response to a potential drift [5]. Moreover, SCs are regarded as feasible candidates for high-power SIBs, due to their high electric conductivity and ease in their interlayer distance tunability [5,9,10]. On the other hand, disordered carbons are crucial in development of all-carbon hybrid ion capacitors (e.g., Li or Na ion capacitors), where high specific powers in the range of 15 to 20 $kW{\cdot}kg^{-1}$ are achievable (ca. one order of magnitude higher than the conventional LIBs) [11]. Accordingly, significant attention has been drawn in screening possible precursors for the soft carbons and their employment and improvement as SIB or hybrid capacitor anode electrodes, especially in the past lustrum [12–18]. These attempts include study of a large number of precursors including pitch [19], petroleum coke [20], mesitylene [21], naphtalenetetracarboxylic dianhydride (NTCDA) [22], polymerized acetone [16], and cellulose nanocrystals [13]. Despite the interesting results and relatively improved electrochemical properties in the previous reports (e.g., a high specific capacity of 359 $mAh{\cdot}g^{-1}$ in the case of polymerized acetone, but with a very low first-cycle coulombic efficiency (FCCE) of 34% [16], or a moderate capacity of 184 $mAh{\cdot}g^{-1}$ with a high FCCE of 80% for perylene tetracarboxylic dianhydride (PTCDA)-derived SC [10]), finding low-cost and applicable precursors/processes to pave the path towards soft carbons with overall improved sodium (and/or lithium) storage properties yet to be realized. This originated from the fact that the (micro)structure of a pyrolytic carbon depends strongly on the nature of the precursor, as well as the pyrolysis parameters (temp., heating rate, gas flow, etc.). This is later translated into the electrochemical signature of the carbon product [4].

Vinyl polymers are one of the largest polymer families, which include the most common type of plastics. A large variety of vinyl polymers can be achieved by replacing hydrogens in the $-CH_2CH_2-$ monomer by heteroatom-containing functional groups. Many of them have been already commercialized, are available with a low-cost (especially polyvinyl chloride, PVC), have been employed in various applications, and their waste products can be used for making carbons. As a matter of fact, the type and the extent of the substitutes dictate the structure and properties of the polymer itself and the carbon achieved via pyrolysis. For instance, the substitution of one H with chlorine will result in polyvinyl chloride, the third-most widely produced synthetic plastic which is popular for its capability of being formed in any shape, while replacing two H with Cl will give polyvinylidene chloride (PVDC) which is a remarkable chemical resistant material. Interestingly, pyrolysis of these two polymers achieves completely different carbons. The one resulted from the H-rich monomer (PVC) is a graphitizable or soft carbon, while the other one cannot form long-range ordered structure and results in a non-graphitizable or hard carbon [23,24]. Despite their small, and not always clear, structural differences (which may be conferred from X-ray diffraction (XRD) patterns (esp. ≤1000 °C)), SCs and HCs thoroughly differ in microstructural aspects [4]. Unlike HCs in which cross-linkers and non-hexagonal polygons prevent their extended/long-range ordering even at high temperatures (c.a. >2500 °C), moderately high pyrolysis temperatures (e.g., up to 1000 °C) will drive graphitizing carbons to relatively large crystalline parallel stacked graphene layers in both basal and interplanar directions. Among all of the vinyl polymer family, PVC is the member whose carbonized residue has been evaluated as a soft carbon for sodium storage applications and showed a capacity of around 200 $mAh{\cdot}g^{-1}$, with an average oxidation potential of 0.5 V vs. Na/Na+ and an FCCE of around

65% [25,26]. This is noteworthy that PVC pyrolysis releases toxic HCl gas and other possible precursor alternatives with more benign products can be of high interest.

In this work, we studied the pyrolysis and carbonization of four simple vinyl polymers, including polyvinyl alcohol (PVA), polyvinyl acetate (PVAc), polyvinyl butyral (PVB), and PVC with the aim of preparing soft carbons. The pyrolysis and carbonization processes were studied through thermo-gravimetrical analysis, and the physicochemical properties of the obtained carbons have been revealed and compared via various characterization methods like powder X-ray diffraction (PXRD) and scanning electron microscopy (SEM). The electrochemical properties of the as-prepared samples were investigated in a three-electrode configuration using carbonate-based electrolyte, and the sodium-storage properties of the vinyl polymer-based SCs were evaluated and compared. In addition, the electrochemical performance of the PVC-derived soft carbon was examined in full-cell hybrid capacitors, demonstrating their promising properties as negative electrodes for high-power applications. This work not only contrasts the carbonization products of several vinyl polymers with neat physicochemical characterization, but also screens potential precursors for soft carbons with interesting storage properties for SIBs and hybrid capacitors. This can pave the path for further research and efforts to improve the electrochemical properties of soft carbons as a potential anode material for energy storage applications.

2. Materials and Methods

2.1. Synthesis of the Soft Carbon Samples

The soft carbon precursors, polyvinyl alcohol (PVA, Mw: 89,000–98,000, 99+% hydrolyzed), polyvinyl acetate (PVAc, Mw: ~100,000), polyvinyl butyral (PVB), and polyvinyl chloride (PVC, low molecular weight) were all purchased from Sigma-Aldrich (St. Louis, MO, USA). Soft carbons were synthesized through pyrolysis of the corresponding polymers (PVA, PVAc, PVB, and PVC) at a temperature of 800 °C, in a tubular furnace under Ar atmosphere. In a typical pyrolysis procedure, the commercial precursor (~4.0 g) was placed in an alumina crucible boat, located in a quartz tube and heated with a rate of 10 °C·min^{-1} up to 110 °C for a dwell-time of 1h, followed by further temperature elevating up to 800 °C with 1 °C·min^{-1} where the temperature was maintained for another hour. The obtained solid product was manually ground in an agate mortar after being naturally cooled down to room temperature (RT). The achieved fine dark powder was then utilized for the characterizations or electrode preparation. The yield of the pyrolysis was calculated by weighing the residue after the thermal treatment. The fine powder in the case of pyrolysis of PVA and PVAc were dispersed in water and ethanol and filtered to wash away possible remained impurities, and the sample was further dried in an electric oven at 120 °C. In order to decrease the particle sizes and evaluate its effect on electrochemical performance of the material, a sample was prepared by mechanical treatment of the PVC-derived soft carbon (PVC-C-BM). For this purpose, a PULVERISETTE 5 planetary mill has been used for 2 h (four 30-min cycles, with 5-min pauses between each cycle) at 250 rpm, using 10 mm zirconium oxide beads (bead to the material ratio of 20:1).

2.2. Characterizations

Powder X-ray diffraction (PXRD) was conducted on a *Bruker D8* diffractometer with monochromatic Cu $K_{\alpha 1}$ (λ = 1.5406 Å) source and LYNXEYE-XE detector in the *Bragg-Brentano* reflection geometry. In order to minimize any background, monocrystalline Si sample holders with shallow well were employed for all of the PXRD measurements.

Thermogravimetrical properties of the polymers were probed from room temperature up to 800 °C using an *STA 449 F3 Jupiter, Netzsch* instrument with an Ar carrier gas.

Scanning electron micrographs (SEM) were captured using an FEI Quanta 200 microscope equipped with *Field Emission* gun and ET detector working at 20 kV accelerating voltage and a spot size of 3.5 nm. The particle size of the samples was approximated by analyzing the SEM images using *ImageJ* software.

2.3. Electrochemical Characterizations

The electrodes were composed of as-prepared soft carbon samples as the active material, carbon additive (Super C65, IMERYS, Paris, France), and polyvinylidene fluoride (PVdF, Alfa Aesar, Alpha, NJ, USA) as the binder with a mass ratio of 90:5:5. A homogeneous slurry was obtained by mixing the electrode materials (300 mg in total) and at least 400 µL of *N-Methyl-2-pyrrolidone* (NMP, Sigma-Aldrich) using a vibratory mixer (SPEX Sample Prep. 8000M) in a 45 mL stainless steel (SS) jar and 3 SS beads with a diameter of 2.5 mm. The slurry was cast onto cleaned Cu foil with a blade height of 150 µm, dried at 120 °C under vacuum overnight in an electric oven, and pressed with a pressure of 2 ton·cm^{-2}. For the SIBs experiments, three-electrode Swagelok cells were assembled with laminated Na metal disks as the counter (CE) and reference electrodes (RE), glass-fiber membrane as the separator (Whatman^{TM} GF/D), and 1 M $NaClO_4$ in EC:PC (1:1 wt.%) (all from Sigma-Aldrich) as the electrolyte in a Ar filled glovebox (O_2 < 0.1 ppm; H_2O < 0.1 ppm). The active material mass loading was ranging from 2 to 4 mg·cm^{-2} depending on the precursor. All the electrochemical measurements were carried out in constant current (galvanostatic) mode on multichannel *VMP3 Bio-Logic* stations at RT where the cells were cycled between 0.002 and 2.0 V versus Na/Na$^+$. In the case of lithium cells, the PVC-C-BM (BM stands for ball milled) has been evaluated in two-electrode half-cells using Li chips as the counter electrode and 1 M $LiPF_6$ in EC:DMC as the electrolyte (LP30 from Solvionic, Toulouse, France). For the Li hybrid capacitors, PVC-C-BM was used as the negative electrode in integration with activated carbon (YP80F AC) as the positive electrode with a mass ratio of 2:1. The LP30 solution was also used as the electrolyte, and these experiments were conducted in a three-electrode configuration, while a Li chip served as the reference to monitoring each electrode individually. Prior to the experiments, cathode and anode were pre-cycled using the Li reference electrode as a counter electrode (2-electrode connection), with anode discharged to 0.2 V and AC charged to 4.2 V. In both Li and Na cells, the C-rate is based on the theoretical capacity of graphite, C = 372 mAh·g^{-1}).

3. Results and Discussion

In order to track the pyrolysis procedure, thermo-gravimetrical behavior of the polymers was studied using TGA, shown in Figure S1. As is seen, the overall mass change of all polymers occurs before 500 °C and all samples depict a similar two-step mass loss profile consisting of one below 350 °C and another at higher temperatures, correlating to the fact that firstly the functional groups attached to the backbone are detached (e.g., deacetylation, dehydroxylation, or dechlorination), and later the polyolefinic backbone disintegrates. The observed thermogravimetrical behavior for all the polymers agrees with the previous reports [27–30]. This thermal decomposition is schematically illustrated in Figure 1, in which during the pyrolysis of a thermoplastic polymer, the solid precursor passes through a fusion state in which the volatiles (depending on the nature of the precursor) come out gradually; starting by water vapor and carbon dioxide (PVA, PVAc, PVB) or HCl (e.g., in the case of PVC), resulting from cleavage of heteroatom-containing functional groups [28,29]. This is later followed by exclusion of other volatiles like CH_4, C_4H_8O (e.g., in the case of PVB) and H_2 originating from dangling atoms/branches. The fusion state allows the carbon backbone to progressively densify, to reorder itself as stacked graphenic layers, and results in the formation of relatively large crystalline parallel stacked graphene layers in both basal and interplanar directions [23,24]. The higher the pyrolysis temperature is elevated, the more H_2 molecule is expelled, leading to extension of the long-range ordering and shrinkage of the interplanar distance [4]. This, along with the order and extent of exclusion originating from the intrinsic chemistry of the precursor, is the origin of the interplanar distance range usually seen in the soft carbons (e.g., 3.4 ≤ d_{002} ≤ 3.6 Å).

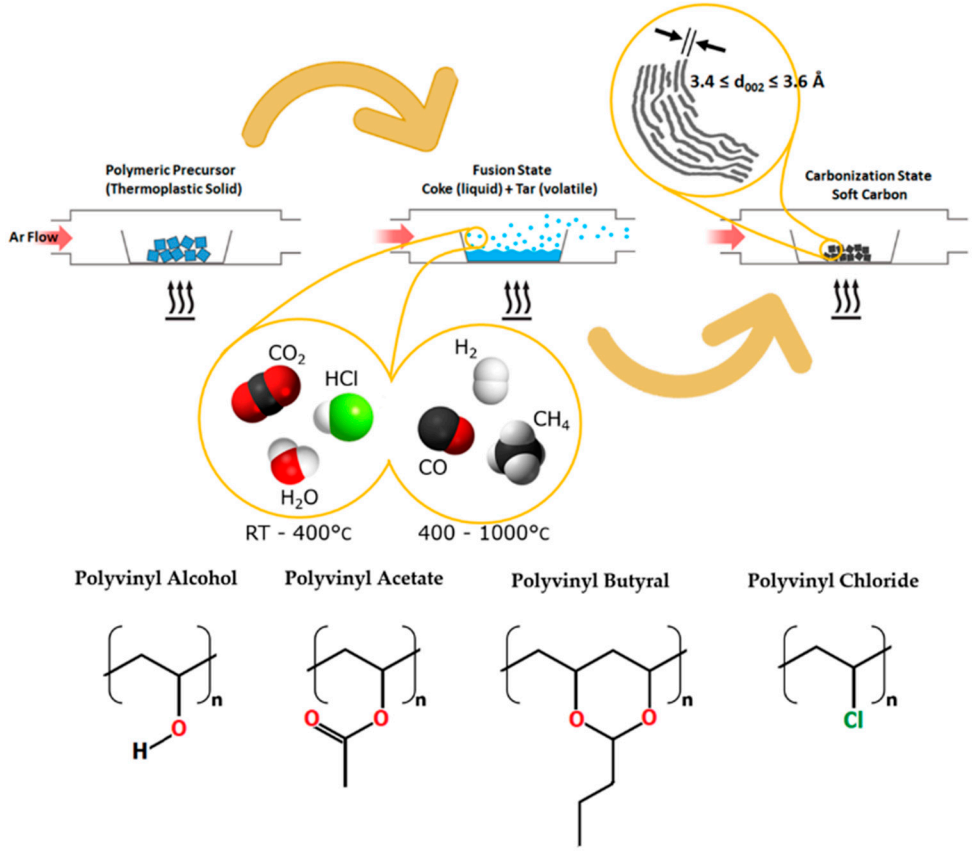

Figure 1. Schematic illustration for pyrolysis of a thermoplastic polymer, resulting in the exclusion of volatiles in various stages and formation of soft carbon with large local crystalline parallel graphene layers; and repeating unit in different polyvinyl family members studied in this work. The C_4H_8O as the expelled gas (e.g., in the case of PVB) is not shown for the sake of simplicity.

The structural properties of the as-prepared samples were probed via powder X-ray diffraction (PXRD), and the diffracted patterns can be seen in Figure 2a. It should be mentioned that patterns recorded right after the pyrolysis of PVA and PVAc depict several sharp but low-intense peaks, evidencing the presence of inorganic impurities in the obtained carbon, possibly originating from the quartz tubes, see Figure S2. Accordingly, the ground powder acquired by pyrolysis of these two polymers were dispersed in distilled water and ethanol, respectively and thoroughly rinsed several times. As seen in Figure 2a, this resulted in a clean PXRD pattern for PVA-derived carbon, while the impurities can yet be seen for the one achieved from PVAc. This can be attributed to the impurities trapped inside the carbon matrix (hence, not being washed away) which is further aggravated by the small yield of the pyrolysis (see Table S1). Moreover, it can be seen that all of the samples show a relatively broad and low intense peak with an almost similar (002) peak position and shape, except in the case of PVA, in which the peak appeared in lower 2θ angles with an apparent larger width. In order to accurately compare the peak characteristics of different samples, the collected XRD patterns were corrected by Lorentz, polarization and illuminated sample volume factors [6], as shown in Figure S3. As it is seen in Figure S3, the (002) and (100) reflections are fitted with Voigt peak functions, and the results for peak position and broadenings are summarized in Table 1. It is noteworthy to mention that in the case of (002) peak, the Gaussian broadening was converging into 0. Accordingly, the (002) peak for all of the sample is centered in a narrow range of 2θ = 25.3–25.5°, corresponding to an interplanar distance of $d_{002} \approx 3.50$ Å, except in the case of carbon prepared from PVA. For PVA-derived carbon, the (002) peak appeared at lower angles (2θ~24.5°), implying a higher interlayer distance (3.64 Å). The obtained interlayer distance demonstrates the soft characteristics of the prepared carbons

(which their d_{002} is normally in the range of 3.4–3.6 Å). However, it should be mentioned that the slightly increased d_{002} of the PVA-C sample may refer to its intermediate character (between soft and hard carbons). In addition, as it can be noted from the Lorentzian width values listed in Table 1, the (002) peak in PVA-C sample is much broader than the others. Pure Lorentzian contribution suggests that the peak broadening mainly arises from second order distortions, i.e., curved or crumpled layers rather than finite crystallite size, which usually causes a prominent Gaussian contribution [31,32].

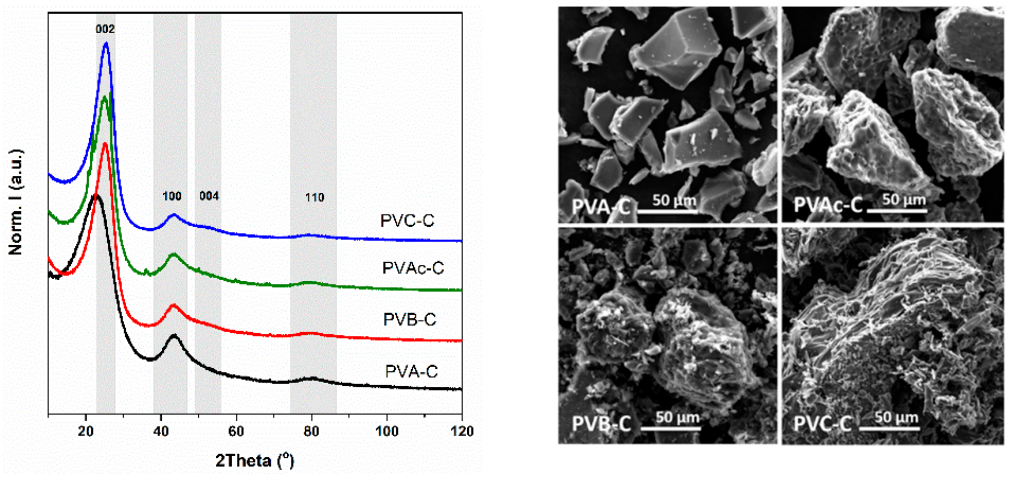

(**a**) (**b**)

Figure 2. Structural and morphological characterization of the prepared soft carbons: (**a**) PXRD patterns of the pyrolyzed polymers at 800 °C under Ar atmosphere; and (**b**) scanning electron micrographs of various samples at a magnification of 1.2 kx.

Table 1. The calculated parameters from the fitting of the corrected powder X-ray diffraction (PXRD), shown in Figure S3.

Sample	$\rho_{struct.}$ ($g \cdot cm^{-3}$) [a]	$2\theta_{002}$ (°)	d_{002} (nm)	WL_{002} (nm^{-1}) [b]	WG_{002} (nm^{-1}) [c]	$2\theta_{100}$ (°)	d_{100} (nm)	WL_{100} (nm^{-1})	WG_{100} (nm^{-1})
PVA-C	2.229	24.492	0.364	7.285	0	43.795	0.207	1.851	2.811
PVAc-C	2.328	25.316	0.352	4.386	0	44.051	0.206	1.462	3.817
PVB-C	2.331	25.397	0.351	4.298	0	44.002	0.206	2.268	3.231
PVC-C	2.343	25.522	0.349	3.973	0	44.016	0.206	1.265	3.930
PVC-C-BM	2.252	25.563	0.348	4.174	0	43.798	0.207	0	3.864

[a] Structural density: $\rho_{struct.} = \rho_{graphite}\left(\frac{d_{002}^{graphite}}{d_{002}}\right)\cdot\left(\frac{d_{100}^{graphite}}{d_{100}}\right)^2$, where $\rho_{graphite}$, $d_{002}^{graphite}$ and $d_{100}^{graphite}$ are structural density, the interlayer and in-plane distance of highly crystalline graphite, respectively; [b], the Lorentzian, and [c], the Gaussian factor of the fitted peaks.

The morphological properties of the prepared samples were evaluated through scanning electron microscopy (SEM). As is seen in Figure 2b and Figure S4, the samples pyrolyzed from PVA and PVAc consist of larger particles compared to the other ones. In the case of PVA-C, the sample is comprised of the particles with a smooth surface, sharp edges (e.g., as result of conchoidal fracture) and with an extended range of particle sizes from a few ten (ca. 12.0) to around 300 µm. The particles of PVAc-C sample are much rougher in the surface, as seen in Figure 2b. In the case of PVB-C and PVC-C samples, although large particles can also be seen in a low magnification (Figure S4), the majority of them are small splinters scattered on bigger particles. In the case of PVC-derived carbon, the sample is comprised of smaller particles in average, and as it can be realized in the magnified micrograph in Figure 2b, each particle has a rough surface (unlike the PVA-derived carbon), and it seems being made up of stacked layers. This is in consistence with the observed PXRD results in which appearance of a broader (002) peak at relatively lower angles suggests a higher degree of structural disorder

(e.g., the smaller radius of layer curvature) or reduced crystallinity in the case of the carbon obtained from PVA in comparison with the rest of the soft carbons, and therefore, a more isotropic appearance at the mesoscale.

The sodium storage capability of the as-prepared soft carbons was tested through constant current charge-discharge (galvanostatic) measurements in a three-electrode configuration in 1 M $NaClO_4$ in EC:PC electrolyte. The voltage-composition profiles of the three polyvinyl-derived soft carbons are displayed in Figure 3a. As can be seen, the PVB-derived carbon shows the largest irreversible capacity, resulting in a smaller FCCE value (e.g., 56%), due to vaster formation of solid electrolyte interface (SEI) among all the other samples; where PVC-derived carbon stands out with an FCCE of 70%. According to the TGA-QMS analysis presented in Figure S5, the release of heteroatom-containing gases occurs for all carbons within the range 250–500 °C, thus ending well below the final carbonization temperature of 800 °C. Heteroatoms are, thus, probably not present in significant amount in the final carbon. Only hydrogen is expected to be still present as H_2 release is detected until the end of the carbonization process. This suggests that the difference in FCCE might not be related to differences in surface chemistry, but rather differences of surface texture. Indeed, as can be seen in Figure S5, the released gases differ depending on the precursor, whose interaction with the carbon residue might lead to different surface texture—CO_2 released by PVA and PVB (see Figure S5) for instance is a known activation agent. A reversible specific capacity (e.g., the capacity per gram of the active material during Na^+ release) of 160, 195, and 212 $mAh{\cdot}g^{-1}$ was recorded for PVA-, PVC-, and PVB-derived SCs, respectively. As shown in Figure 3b, the Na^+ uptake/release profiles of all samples essentially exhibit a sloping voltage, without extended low-voltage plateau (usually seen for HCs)—which is a typical signature of soft carbons [33]. This can be further seen in the derivative curves, shown in Figure 3c.

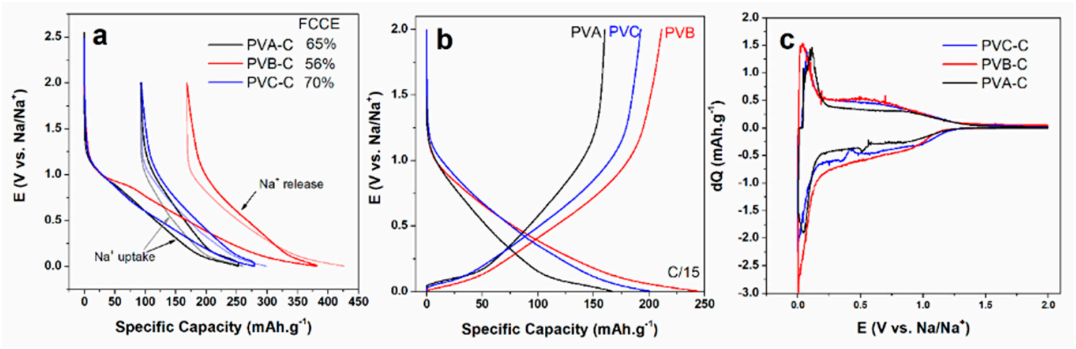

Figure 3. The sodium storage capability of the polyvinyl-derived soft carbons in a three-electrode configuration in 1 M $NaClO_4$ in EC:PC solution: (**a**) (Dis)charge profiles of the sample at C/15 (C = 372 $mA{\cdot}g^{-1}$); (**b**) second (dis)charge profiles of the samples; and (**c**) derivative curve, dQ vs. potential, of the samples at C/15.

Furthermore, the rate capability of the samples was probed through cycling the cells at various current loads for five consecutive cycles in each load (Figure S6), and the results based on the fifth cycle in each rate (e.g., ranging from C/15 to 10C) are plotted in Figure 4a. As it can be seen, PVC-derived carbon outperformed the other cells at higher current loads (up to 5C), delivering a capacity of 100 and 50 $mAh{\cdot}g^{-1}$ at currents of 0.75 and 1.9 $A{\cdot}g^{-1}$, respectively. After 40 consecutive cycles at various specific currents, the cells were cycled at C/15 up to 55 cycles (Figure S6). As can be seen, the initial reversible capacity of the cells has been recovered, and the PVA-C and PVC-C samples exhibit stable performance. Although PVB-derived carbon has the highest initial capacity at low current densities, its specific capacity fades faster in comparison with the other two samples. This is more evident in long cycling at C/15, as shown in Figure S7. This can be correlated to PVB-C's poorer coulombic efficiency below 95% (compared to nearly 100% for PVC-C), suggesting non-stable SEI or the presence of a side reaction.

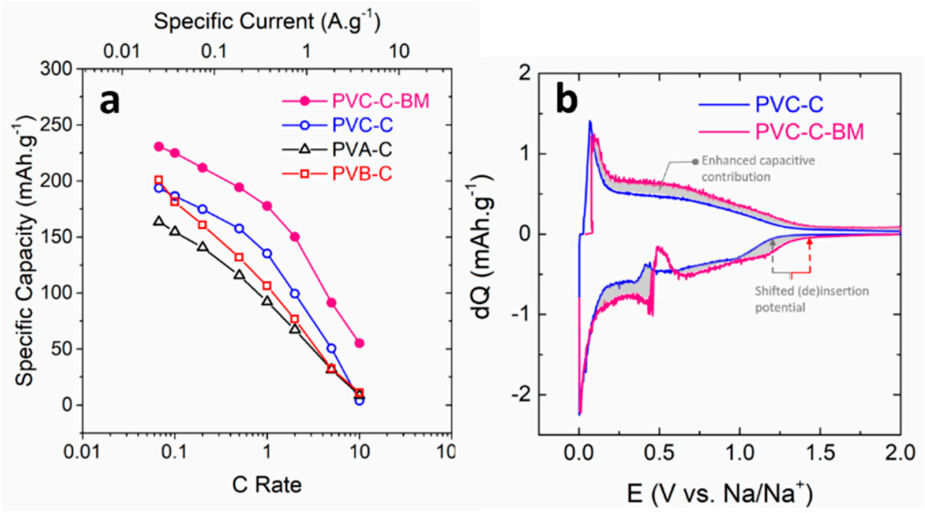

Figure 4. (**a**) Rate capability (based on Q_{rev} in the fifth cycle of each load) of the polyvinyl-derived soft carbons at various current loads ranging from C/15 to 10C; and (**b**) derivative curve, dQ vs. potential, of the PVC-derived soft carbons (BM stands for ball-milled) at C/15, (C = 372 mA·g^{-1}).

It is already known that increasing the specific surface area of the carbon materials (e.g., by decreasing the size of the particles) can enhance their capability to store alkali ions (e.g., Na^+ and Li^+), especially for high-power applications. Accordingly, with the aim of evaluating and enhancing the performance of the PVC-C soft carbon, especially at higher C-rates, a PVC-C sample has been ball-milled, PVC-C-BM hereafter. As it is shown from the SEM images and the particle size distribution depicted, respectively, in Figure S8 and S9a, the particles have been significantly reduced in size, compared to the sample without ball-milling (PVC-C, see Figure 2b). This resulted in an almost 10-fold increase in the specific surface area obtained from N_2 gas physisorption (e.g., 38 $m^2 \cdot g^{-1}$ for PVC-C-BM against 3.9 $m^2 \cdot g^{-1}$ for not treated sample, PVC-C; see isotherms in Figure S9b), originating from the extended porosity of the sample through ball-milling, as shown by estimated pore size distribution via non-local density functional theory, NLDFT (Figure S9c). Such a mechanical treatment resulted in a significantly enhanced population of the micropores centered at ~1 nm, leading to specific capacity enhancement of 28% (ca. 250 mAh·g^{-1}) at C/15 (see Figure S10a), compared to PVC-C sample. This enhanced charge storage capacity can be attributed to the augmented amount of the accessible active material to the electrolyte (which consequently increases the capacitive contribution), as well as apparent shifted (de)insertion potential as realized in Figure 4b. However, such an improved capacity comes at the expense of a reduced FCCE of 50% (against 70% for PVC-C). The coulombic efficiency deterioration can be indeed attributed to the fact that the SEI formation would consume more charges with the enhanced surface area of the particles in contact with the electrolyte. On the other side, the PVC-C-BM outperformed the non-treated sample in terms of the reversible specific capacity at various current loads (displayed in Figure 4a), providing a high capacity of 55 mAh·g^{-1} at 10C. Such an excellent rate capability for the PVC-C-BM sample can be correlated to the shortened charge carrier diffusion path in response to enhanced specific surface area and porosity character of the carbon sample (see Figure S9c).

According to the obtained results, the vinyl polymers (especially PVB and PVC) are indeed promising precursors for SCs, compared to more traditional soft carbons, such as carbonized Petroleum Coke or Coal tar Pitch [7]. Figure 5 shows an overview of the electrochemical storage performance (e.g., projected specific energy/FCCE vs. specific capacity) of the previously reported soft carbons in comparison with the polyvinyl-based SCs studied in this work (see Table S2 for the detailed information). As can be seen, the polyvinyl-based SCs studied here are amongst soft carbons with the highest extrapolated specific energy in a full cell (considering the integration with *Faradion* layered oxide as a state-of-the-art cathode material) ranging in 220–255 Wh·kg^{-1}. These values are far better than

commercial LIB technologies based on lithium titanate anode (LTO), although there is a need for this to be further improved in order to compete with technologies like Graphite-$LiMn_2O_4$ (G-LMO). Moreover, a significant decrease in FCCE can be distinguished beyond specific capacities of 200–250 mAh·g^{-1}, originating mainly from either larger voltage hysteresis or extended SEI formation (as a result of high SSA, e.g., in the case of PVC-C-BM). Therefore, further studies to achieve high-performance soft carbon materials without sacrificing coulombic efficiency seem crucial in order to turn them into a viable solution for high-performance SIBs, an issue which is under investigation and will be addressed in future reports.

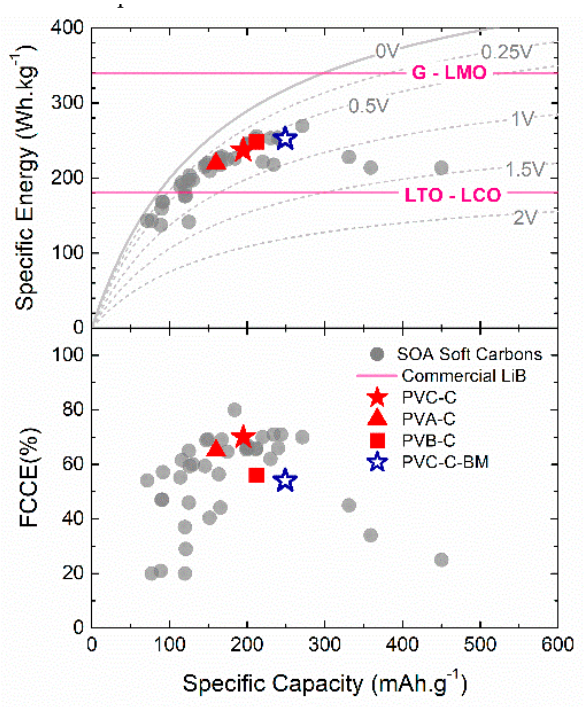

Figure 5. Overall performance (specific energy and first-cycle coulombic efficiency (FCCE) against specific capacity, top and bottom panels, respectively) comparison of the state-of-the-art (SOA) reported soft carbons (see Table S2 for details), and the polyvinyl-based SCs studied here. The specific energy has been calculated by considering the total mass of the active materials (both cathode and anode) and employment of the *Faradion* layered oxide as the cathode (mAh·g^{-1} at 3.2 V). Commercial Li-ion cell based on $Li_4Ti_5O_{12}$-$LiCoO_2$ (LTO-LCO) and graphite-$LiMn_2O_4$ (G-LMO) with moderate specific energy at active materials is represented for the sake of comparison.

Based on the favorable high-power performance seen for the PVC-C-BM sample, the applicability of the sample has been further evaluated as an anode electrode in integration with an activated carbon (Kuraray YP80F) in hybrid Li-ion capacitor devices. To this end, firstly Li storage performance of the PVC-C-BM sample has been evaluated, and the results are shown in Figure 6a,b. As it is seen, the sample stored around 300 mAh·g^{-1} at C/15 (after stabilization), and a capacity retention of around 20% (e.g., ~60 mAh·g^{-1}) with an increase of 150-fold of the specific current to 10C. These results are comparable with LTO used for high-power Li-ion batteries (e.g., ~75 mAh·g^{-1} at 10C for LTO or TiO_2 nanowires in Reference [34]), demonstrating the PVC-based soft carbons as promising candidates for high-power applications. However, it should be reemphasized that their low initial coulombic efficiency must be addressed for any practical use [35]. Figure 6c depicts the first five charge-discharge cycles of the full-cell hybrid Li-ion capacitor, as well as those of the individual electrodes collected against the Li metal reference, at a specific current of 1 A·g^{-1}. As it is seen, the charge/discharge profiles of the full-cell are comprised of nearly symmetric triangular-shaped cycles despite the extended voltage window between 1.5 to 4.2 V vs. Li/Li^+ and the high applied specific current of 1 A·g^{-1} ($t_{discharge}$ = 81 s),

revealing reversible nature of the governing reactions. During the cycles, cathode and anode swing in the range of 2.23–4.55 V and 0.34–0.73 V vs. Li/Li^+, respectively. Furthermore, Figure S11a shows the evolution of the specific capacitance of the PVC-C-BM//AC hybrid capacitor in various specific currents ranging from 0.05 to 5 $A{\cdot}g^{-1}$, demonstrating a capacitance retention of 70% (25 $F{\cdot}g^{-1}$) after a 100-fold increase of the current to 5 $A{\cdot}g^{-1}$. The charge/discharge profiles in some selected specific currents are also shown in Figure S11b–d, revealing almost intact triangular shape with a marginal increase in the ohmic drop up to 3 $A{\cdot}g^{-1}$ (where the enhanced ohmic drop can be realized), suggesting high power characteristic of the assembled device. Figure 6d depicts the *Ragone* plot, based on the sum of the active mass of both electrodes, for the PVC-C-BM//AC hybrid Li capacitor in comparison with a double layer capacitor device (EDLC) comprised of two symmetrical electrodes (activated carbon, YP80F). As can be seen, the hybrid could attain a maximum specific energy of ca. 73 $Wh{\cdot}kg^{-1}$ at a specific power of 28 $W{\cdot}kg^{-1}$. This is over three times greater than the maximum energy of a symmetric EDLC device (e.g., 22 $Wh{\cdot}kg^{-1}$), and lies well within the reported values for such devices, e.g., References [17,36,37]. In addition, it is noteworthy that the hybrid cell could deliver a maximum specific power as high as 12.5 $kW{\cdot}kg^{-1}$ (e.g., at 5 $A{\cdot}g^{-1}$) against 5.8 $kW{\cdot}kg^{-1}$ for the EDLC at the same specific current. Indeed, hybrid cells are expected to show an increase in energy density compared to pure EDLC cells, at the cost of a decreased power density. Nevertheless, it can be seen that the PVC-C-BM//AC hybrid Li capacitor could deliver a specific power as high as 12.5 $kW{\cdot}kg^{-1}$ at a specific current of 5 $A{\cdot}g^{-1}$, demonstrating its high-power performance (see charge-discharge profiles in Figure S11).

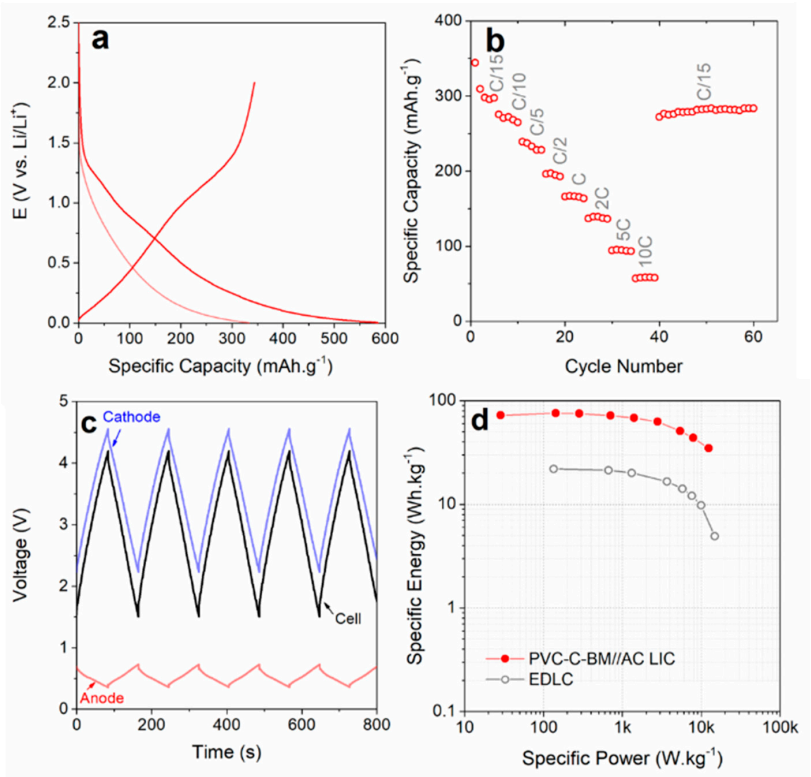

Figure 6. Lithium storage performance of the PVC-derived soft carbon (PVC-C-BM) as the negative electrode for Li-ion battery application (**a**,**b**) and in a hybrid Li capacitor (**c**,**d**). Li-ion battery: (**a**) Two first discharge-charge cycles of the PVC-C-BM sample in 1 M $LiPF_6$ in EC:DMC at C/15 rate; and (**b**) rate capability of the PVC-C-BM sample at various C-rates ranging from C/15 to 10C, (C = 372 $mA{\cdot}g^{-1}$). Hybrid Li capacitor. (**c**) The first five charge-discharge cycle of the PVC-C-BM//AC Li ion capacitor (LIC) at a specific current of 1 $A{\cdot}g^{-1}$; and (**d**) Ragone plot of the hybrid capacitor compared to a symmetrical AC-based capacitor (EDLC); the values are based on the sum of the mass for both electrodes.

All the obtained electrochemical properties demonstrated the potential applicability of vinyl polymers as soft carbon precursors for energy storage applications. XRD data confirmed that the microstructural feature of such carbons is mainly originated from distorted sp^2 carbon layers, shown by large Lorentzian contribution in diffracted peaks. This is in agreement with previous reports for typical soft carbons derived from PeC [17,32], and with the observed disordered bent layered structures in non-graphitic carbon via high-resolution transmission electron microscopy [38]. The electrochemical signature of such carbons agrees with what has been already reported for soft carbons, and contrasts hard carbon typical electrochemical behavior (e.g., including both the sloping and low-voltage plateau regions). In summary, the vinyl polymer family members studied here demonstrated promising storage properties when carbonized into soft carbons (i.e., PVC and PVB). The storage capability of such carbons could be further optimized, as exemplified by enhanced charge storage and rate capability in PVC-C-BM sample; yet further solutions and approaches are in high demand to improve the initial coulombic efficiency as well. Such approaches would be addressed in our future reports.

4. Conclusions

In summary, the pyrolysis carbon products of four various precursors belonging to vinyl polymer family were characterized via different physicochemical methods, including PXRD, SEM, and TGA. The obtained results demonstrated that the products possess soft carbon properties, and their structural characteristics were compared. The pyrolysis yield for polyvinyl alcohol and polyvinyl acetate was found to be too smalls and needs to be improved for any practical applications. The careful XRD analyses shed light on (micro)structural properties of the as-prepared carbons, revealing the existence of curved/crumpled sp^2 carbon layers. The electrochemical properties of the obtained soft carbons were evaluated in the carbonate-based electrolyte, and the results show their promising behavior for sodium ion storage applications. Accordingly, polyvinyl butyral (PVB)-derived soft carbon showed the highest reversible capacity of 212 $mAh{\cdot}g^{-1}$ vs. sodium. Moreover, the PVC-based carbon outstood the other soft carbons in terms of coulombic efficiency in the first cycle (70%). Overall, PVB and PVC look promising soft carbon precursors which are worth further study to tune their electrochemical properties. In addition, the obtained results showed promising results for the use of such soft carbons in hybrid capacitors. All these are of high importance and interest, due to the low-cost and common use of these polymers in various industries, which make potentially their waste a valuable source for soft carbon precursors with energy storage applications.

Supplementary Materials: The following are available online at http://www.mdpi.com/1996-1073/13/16/4189/s1, including: TGA; PXRD of PVA and PVAc before washing; corrected PXRD profiles; SEM; Rate Capability vs. Na; N_2 gas physisorption isotherms and corresponding analysis; EC properties of PVC-C-BM; EC properties of the LIC hybrid device; Tables S1 and S2.

Author Contributions: Conceptualization, D.S.; Experiments, A.P., B.O., J.A., M.J.; Data curation, A.P., J.A.; formal analysis, A.P., B.O., J.A.; Writing—original draft preparation, A.P.; Writing—review and editing, A.P., J.A., D.S.; Supervision, D.S.; Funding acquisition, D.S. All authors have read and agreed to the published version of the manuscript.

Funding: The authors gratefully thank the financial support of the Ministerio de Economía y Competitividad through AffINITy grant (ENE2016-75242-R), the Ministerio de Ciencia e Innovación through NIB-MOVE grant (PID2019-107468RB-C22) and the Basque Government through ELKARTEK projects CICE17 and CICe2020 (KK 2020/00078).

Acknowledgments: We gratefully acknowledge Skye Clarke whose efforts and results inspired significant parts of the current work.

Conflicts of Interest: The authors declare no conflict of interest.

References

1. Yabuuchi, N.; Kubota, K.; Dahbi, M.; Komaba, S. Research Development on Sodium-Ion Batteries. *Chem. Rev.* **2014**, *114*, 11636–11682. [CrossRef] [PubMed]
2. Ángel, M.-M.M.; Damien, S.; Luis, G.-C.J.; Montse, C.-C.; Elizabeth, C.-M.; Teófilo, R. Na-Ion Batteries for Large Scale Applications: A Review on Anode Materials and Solid Electrolyte Interphase Formation. *Adv. Energy Mater.* **2017**, *7*, 1700463.
3. Kim, S.-W.; Seo, D.-H.; Ma, X.; Ceder, G.; Kang, K. Electrode Materials for Rechargeable Sodium-Ion Batteries: Potential Alternatives to Current Lithium-Ion Batteries. *Adv. Energy Mater.* **2012**, *2*, 710–721. [CrossRef]
4. Saurel, D.; Orayech, B.; Xiao, B.; Carriazo, D.; Li, X.; Rojo, T. From Charge Storage Mechanism to Performance: A Roadmap toward High Specific Energy Sodium-Ion Batteries through Carbon Anode Optimization. *Adv. Energy Mater.* **2018**, *8*, 1703268. [CrossRef]
5. Yao, X.; Ke, Y.; Ren, W.; Wang, X.; Xiong, F.; Yang, W.; Qin, M.; Li, Q.; Mai, L. Defect-Rich Soft Carbon Porous Nanosheets for Fast and High-Capacity Sodium-Ion Storage. *Adv. Energy Mater.* **2019**, *9*, 1803260. [CrossRef]
6. Dou, X.; Hasa, I.; Saurel, D.; Vaalma, C.; Wu, L.; Buchholz, D.; Bresser, D.; Komaba, S.; Passerini, S. Hard carbons for sodium-ion batteries: Structure, analysis, sustainability, and electrochemistry. *Mater. Today* **2019**, *23*, 87–104. [CrossRef]
7. Doeff, M.M.; Ma, Y.; Visco, S.J.; DeJonghe, L.C. Electrochemical Insertion of Sodium into Carbon. *J. Electrochem. Soc.* **1993**, *140*, L169. [CrossRef]
8. Stevens, D.A.; Dahn, J.R. An In Situ Small-Angle X-Ray Scattering Study of Sodium Insertion into a Nanoporous Carbon Anode Material within an Operating Electrochemical Cell. *J. Electrochem. Soc.* **2000**, *147*, 4428–4431. [CrossRef]
9. Luo, W.; Jian, Z.; Xing, Z.; Wang, W.; Bommier, C.; Lerner, M.M.; Ji, X. Electrochemically Expandable Soft Carbon as Anodes for Na-Ion Batteries. *ACS Cent. Sci.* **2015**, *1*, 516–522. [CrossRef]
10. Jian, Z.; Bommier, C.; Luo, L.; Li, Z.; Wang, W.; Wang, C.; Greaney, P.A.; Ji, X. Insights on the Mechanism of Na-Ion Storage in Soft Carbon Anode. *Chem. Mater.* **2017**, *29*, 2314–2320. [CrossRef]
11. Ding, J.; Hu, W.; Paek, E.; Mitlin, D. Review of Hybrid Ion Capacitors: From Aqueous to Lithium to Sodium. *Chem. Rev.* **2018**, *118*, 6457–6498. [CrossRef] [PubMed]
12. Chen, S.; Wang, J.; Fan, L.; Ma, R.; Zhang, E.; Liu, Q.; Lu, B. An Ultrafast Rechargeable Hybrid Sodium-Based Dual-Ion Capacitor Based on Hard Carbon Cathodes. *Adv. Energy Mater.* **2018**, *8*, 1800140. [CrossRef]
13. Zhu, H.; Shen, F.; Luo, W.; Zhu, S.; Zhao, M.; Natarajan, B.; Dai, J.; Zhou, L.; Ji, X.; Yassar, R.S.; et al. Low temperature carbonization of cellulose nanocrystals for high performance carbon anode of sodium-ion batteries. *Nano Energy* **2017**, *33*, 37–44. [CrossRef]
14. Fan, L.; Liu, Q.; Chen, S.; Xu, Z.; Lu, B. Soft Carbon as Anode for High-Performance Sodium-Based Dual Ion Full Battery. *Adv. Energy Mater.* **2017**, *7*, 1602778. [CrossRef]
15. Li, Y.; Mu, L.; Hu, Y.-S.; Li, H.; Chen, L.; Huang, X. Pitch-derived amorphous carbon as high performance anode for sodium-ion batteries. *Energy Storage Mater.* **2016**, *2*, 139–145. [CrossRef]
16. Hou, H.; Banks, C.E.; Jing, M.; Zhang, Y.; Ji, X. Carbon Quantum Dots and Their Derivative 3D Porous Carbon Frameworks for Sodium-Ion Batteries with Ultralong Cycle Life. *Adv. Mater.* **2015**, *27*, 7861–7866. [CrossRef]
17. Schroeder, M.; Winter, M.; Passerini, S.; Balducci, A. On the cycling stability of lithium-ion capacitors containing soft carbon as anodic material. *J. Power Sources* **2013**, *238*, 388–394. [CrossRef]
18. Yun, Y.S.; Cho, S.Y.; Kim, H.; Jin, H.-J.; Kang, K. Ultra-Thin Hollow Carbon Nanospheres for Pseudocapacitive Sodium-Ion Storage. *ChemElectroChem* **2015**, *2*, 359–365. [CrossRef]
19. Song, L.-J.; Liu, S.-S.; Yu, B.-J.; Wang, C.-Y.; Li, M.-W. Anode performance of mesocarbon microbeads for sodium-ion batteries. *Carbon* **2015**, *95*, 972–977.
20. Alcántara, R.; Jiménez Mateos, J.M.; Tirado, J.L. Negative Electrodes for Lithium- and Sodium-Ion Batteries Obtained by Heat-Treatment of Petroleum Cokes below 1000 °C. *J. Electrochem. Soc.* **2002**, *149*, A201. [CrossRef]
21. Pol, V.G.; Lee, E.; Zhou, D.; Dogan, F.; Calderon-Moreno, J.M.; Johnson, C.S. Spherical Carbon as a New High-Rate Anode for Sodium-ion Batteries. *Electrochim. Acta* **2014**, *127*, 61–67. [CrossRef]
22. Li, W.; Zhou, M.; Li, H.; Wang, K.; Cheng, S.; Jiang, K. A high performance sulfur-doped disordered carbon anode for sodium ion batteries. *Energy Environ. Sci.* **2015**, *8*, 2916–2921. [CrossRef]

23. Franklin, R.E.; Randall, J.T. Crystallite growth in graphitizing and non-graphitizing carbons. *Proc. R. Soc. Lond. Ser. A Math. Phys. Sci.* **1951**, *209*, 196–218.
24. Kipling, J.J.; Sherwood, J.N.; Shooter, P.V.; Thompson, N.R. Factors influencing the graphitization of polymer carbons. *Carbon* **1964**, *1*, 315–320. [CrossRef]
25. Bai, Y.; Wang, Z.; Wu, C.; Xu, R.; Wu, F.; Liu, Y.; Li, H.; Li, Y.; Lu, J.; Amine, K. Hard Carbon Originated from Polyvinyl Chloride Nanofibers As High-Performance Anode Material for Na-Ion Battery. *ACS Appl. Mater. Interfaces* **2015**, *7*, 5598–5604. [CrossRef]
26. Stevens, D.A. Mechanisms for Sodium Insertion in Carbon Materials. Ph.D. Thesis, Dalhousie University, Halifax, NS, Canada, 2000. Available online: https://dalspace.library.dal.ca/handle/10222/55814 (accessed on 1 July 2019).
27. Uyar, T.; Tonelli, A.E.; Hacaloğlu, J. Thermal degradation of polycarbonate, poly(vinyl acetate) and their blends. *Polym. Degrad. Stab.* **2006**, *91*, 2960–2967. [CrossRef]
28. Yang, H.; Xu, S.; Jiang, L.; Dan, Y. Thermal Decomposition Behavior of Poly (Vinyl Alcohol) with Different Hydroxyl Content. *J. Macromol. Sci. Part B* **2012**, *51*, 464–480. [CrossRef]
29. Earnest, C.M. *Compositional Analysis by Thermogravimetry*; ASTM International: West Conshohocken, PA, USA, 1988; Volume 997.
30. Dhaliwal, A.K.; Hay, J.N. The characterization of polyvinyl butyral by thermal analysis. *Thermochim. Acta* **2002**, *391*, 245–255. [CrossRef]
31. Vonk, C. The small-angle scattering of distorted lamellar structures. *J. Appl. Crystallogr.* **1978**, *11*, 541–546. [CrossRef]
32. Saurel, D.; Segalini, J.; Jauregui, M.; Pendashteh, A.; Daffos, B.; Simon, P.; Casas-Cabanas, M. A SAXS outlook on disordered carbonaceous materials for electrochemical energy storage. *Energy Storage Mater.* **2019**, *21*, 162–173. [CrossRef]
33. Ajuria, J.; Redondo, E.; Arnaiz, M.; Mysyk, R.; Rojo, T.; Goikolea, E. Lithium and sodium ion capacitors with high energy and power densities based on carbons from recycled olive pits. *J. Power Sources* **2017**, *359*, 17–26. [CrossRef]
34. Liao, J.-Y.; Chabot, V.; Gu, M.; Wang, C.; Xiao, X.; Chen, Z. Dual phase Li4Ti5O12–TiO2 nanowire arrays as integrated anodes for high-rate lithium-ion batteries. *Nano Energy* **2014**, *9*, 383–391. [CrossRef]
35. Arnaiz, M.; Shanmukaraj, D.; Carriazo, D.; Bhattacharjya, D.; Villaverde, A.; Armand, M.; Ajuria, J. A transversal low-cost pre-metallation strategy enabling ultrafast and stable metal ion capacitor technologies. *Energy Environ. Sci.* **2020**. [CrossRef]
36. Leng, K.; Zhang, F.; Zhang, L.; Zhang, T.; Wu, Y.; Lu, Y.; Huang, Y.; Chen, Y. Graphene-based Li-ion hybrid supercapacitors with ultrahigh performance. *Nano Res.* **2013**, *6*, 581–592. [CrossRef]
37. Ren, J.J.; Su, L.W.; Qin, X.; Yang, M.; Wei, J.P.; Zhou, Z.; Shen, P.W. Pre-lithiated graphene nanosheets as negative electrode materials for Li-ion capacitors with high power and energy density. *J. Power Sources* **2014**, *264*, 108–113. [CrossRef]
38. Marsh, P.A.; Voet, A.; Mullens, T.J.; Price, L.D. Quantitative micrography of carbon black microstructure. *Carbon* **1971**, *9*, 797–805. [CrossRef]